Design of a 1 Tb/s Superchannel Coherent Receiver

David S. Millar, *Member, IEEE*, Robert Maher, *Senior Member, IEEE*, Domaniç Lavery, *Member, IEEE*, Toshiaki Koike-Akino, *Senior Member, IEEE*, Milutin Pajovic, *Member, IEEE*, Alex Alvarado, *Senior Member, IEEE*, Milen Paskov, *Member, IEEE*, Keisuke Kojima, *Senior Member, IEEE*, Kieran Parsons, *Senior Member, IEEE*, Benn C. Thomsen, *Member, IEEE*, Seb J. Savory, *Senior Member, IEEE* and Polina Bayvel, *Fellow, IEEE*

(Invited Paper)

***Abstract*—We describe the design of a trained and pilot-aided digital coherent receiver, capable of detecting a 1 Tb/s superchannel with a single optical front-end. Algorithms for receiver training are described, which calculate the equalizer coefficients, subchannel SNRs, and centroids of the transmitted constellations. Algorithms for pilot-aided operation are then described in detail, providing pilot-aided constant modulus equalization and joint carrier phase estimation over several coherent subchannels. We demonstrate detection of a superchannel with net bit rate in excess of 1 Tb/s with a single coherent receiver. An 11×10 GBd DP-64QAM Nyquist superchannel is used, with 1.32 Tb/s gross bit rate.**

I. Introduction

In order to provide higher optical interface rates, recent research has focused on the expansion of both bandwidth and spectral efficiency (SE) [1], [2]. While some research has focused on the slicing of the received signal in the time [3], [4] or frequency [5] domains, these solutions require several parallel coherent receivers. More recently, detection of 1 Tb/s with a single coherent receiver has been demonstrated with several coherent optical carriers being used to synthesize a single-carrier dual-polarization 32-ary quadrature amplitude modulation (DP-32QAM) signal [6], with a DP-32QAM superchannel [7], and with a DP-64QAM superchannel [8].

In understanding the reason for this approach to increasing interface rates, it is useful to examine the progress of products, proposed products, and experimental records over the last several years, a scatter diagram of which is plotted as SE versus bandwidth in Fig. 1. Coherent systems operating at 100 Gb/s have been a technical and commercial success, relaxing optical plant requirements while requiring only around $3\times$ the optical bandwidth of 10 Gb/s intensity-modulation direct-detection (IM-DD) systems. While relatively sophisticated transceiver optics were required for 100 Gb/s systems, the increase in SE that they offered was enabled by the use of sophisticated digital signal processing (DSP). A further increase in SE within the same bandwidth has resulted in products which achieve 200 Gb/s with a single carrier. The subsequent increase to 400 Gb/s with a single transmitter and receiver has proven more technically challenging than may have initially been suspected. While real-time single carrier systems operating at 400 Gb/s have been demonstrated [9], proposed systems are currently still undergoing standardization by the Optical Internetworking Forum (OIF) [10]. The reason for this is, in part, the availability of sufficiently high speed signal convertors for the transmitter. At the time of writing, the best available arbitrary waveform generator (AWG) has 32 GHz of analog bandwidth [11], while the best available real-time digital sampling oscilloscope has 100 GHz [12]. To overcome the bandwidth limits of commercially available transmitter hardware, recent research has therefore focused on the use of several transmitters with lower bandwidth and good noise performance to create a superchannel [13], which is then detected by a single receiver [6]–[8], [14], while optical time division multiplexing has also been investigated [15].

In this paper, we develop our previous work [8] and provide a thorough exposition of the detailed design of receiver DSP capable of detecting a 1 Tb/s superchannel. In section II, we describe the experimental hardware used for generation and detection of a 1 Tb/s superchannel. We then provide an overview of the receiver DSP strategy in section III, before describing the details of the receiver training algorithms in section IV, and pilot-aided algorithms in section V. We then discuss the experimental performance of the various subsystems in section VI, before providing conclusions in section VII.

II. Experimental Setup

The transmitter setup used in this experiment is shown in Fig. 2. An external cavity laser (ECL) with 100 kHz linewidth was used to seed an optical comb generator (OCG), resulting in 11 subcarriers spaced at 10.01 GHz [16]. The OCG consisted of two Mach–Zehnder modulators (MZMs),

Manuscript received October 24, 2015; revised January 1, 2016;

D. S. Millar, T. Koike-Akino, M. Pajovic, K. Kojima, and K. Parsons are with Mitsubishi Electric Research Laboratories (MERL), 201 Broadway, Cambridge, MA 02139, U.S.A. (e-mail: millar@merl.com; koike@merl.com; pajovic@merl.com; kojima@merl.com; parsons@merl.com).

Robert Maher, Domaniç Lavery, Alex Alvarado, Milen Paskov, Benn C. Thomsen, and Polina Bayvel are with University College London (UCL), Torrington Place, London, U.K. (e-mail: r.maher@ee.ucl.ac.uk, d.lavery@ee.ucl.ac.uk, a.alvarado@ucl.ac.uk, m.paskov@ee.ucl.ac.uk, b.thomsen@ee.ucl.ac.uk, p.bayvel@ee.ucl.ac.uk).

S.J. Savory is with the University of Cambridge, Department of Engineering, Electrical Division, 9 JJ Thomson Avenue, Cambridge, CB3 0FA, U.K. (email: sjs1001@cam.ac.uk).

This work was in part funded by the UK EPSRC Programme Grant EP/J017582/1, and the Royal Academy of Engineering/ the Leverhulme Trust Senior Research Fellowship held by S. J. Savory.

Color versions of the figures in this paper are available online at http://ieeexplore.ieee.org.

Digital Object Identifier xx.xxx/JLT.2016.xxx

This article has been accepted for publication in a future issue of this journal, but has not been fully edited. Content may change prior to final publication. Citation information: DOI 10.1109/JLT.2016.2519260, Journal of Lightwave Technology

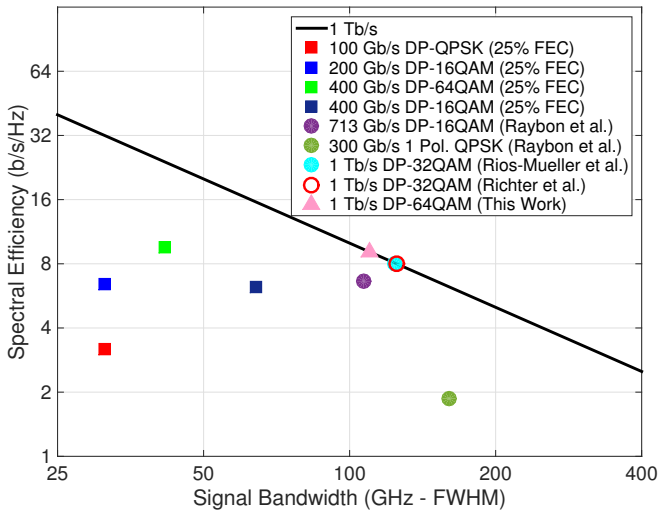

Fig. 1. Background of current products (100 Gb/s and 200 Gb/s), OIF proposals (400 Gb/s) and hero experiments (others).

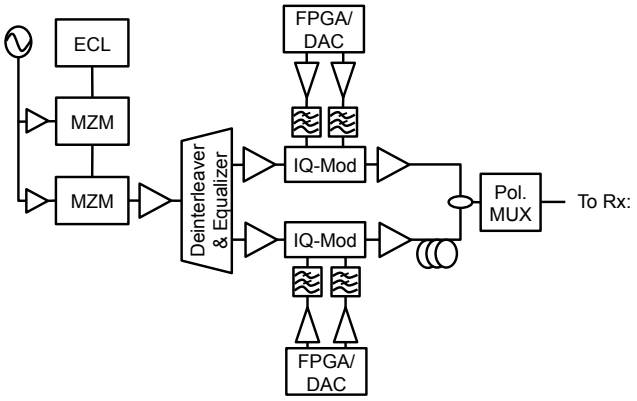

Fig. 2. Experimental setup for 11 subcarrier superchannel transmitter using optical comb generation.

driven with a 10.01 GHz sinusoid. Driving amplitude and bias were tuned along with the sinusoid phase at each modulator in order to achieve a flat optical comb with the required number of subcarriers. The subcarriers were then separated into odd and even channels by cascaded interleavers, before modulation using single polarization I/Q modulators. Two field-programmable gate arrays (FPGAs) were used to send the in-phase and quadrature components of the desired waveforms to a pair of digital-to-analog converters, operating at 20 GSa/s. The 10 GBd, 8-level signals were generated from decorrelated de Bruijn sequences of length 2^{15}, which were filtered with a root-raised-cosine (RRC) finite impulse response (FIR) filter with a roll-off of 10^{-3}. After modulation and decorrelation by 17 ns in the optical domain, the odd and even channels were combined, before passive polarization multiplexing emulation (with delay of 489 symbols).

The receiver setup used in this experiment is shown in Fig. 3. The optical receiver used was a discrete micro-optic 2×8 90° hybrid with 4 unamplified, balanced photodiodes used for detection (with bandwidth 70 GHz). The local oscillator was an ECL with linewidth 100 kHz, tuned to within

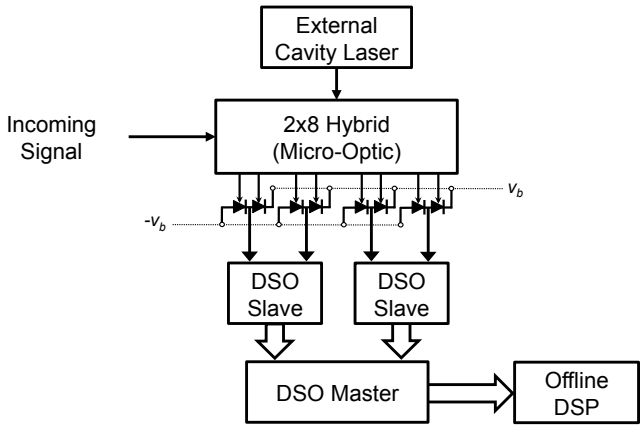

Fig. 3. Experimental setup for ultra-broadband digital coherent optical receiver.

100 MHz of the transmitter seed laser. The electrical signals were digitized using an oscilloscope with 160 GSa/s analog-to-digital converters and 63 GHz of bandwidth, before being processed offline using Matlab.

III. Receiver Digital Signal Processing

In our previous work [17], we noted that the limit of achievable signal-to-noise ratio (SNR) for high order modulated signals was reasonably high, but the use of blind receiver algorithms can cause significant impairments – particularly when the SNR is poor. The receiver DSP design therefore consists of two main components. The receiver was initially operated in training mode in order to estimate the equalizer taps for each of the subchannels, the SNR on each subchannel, and the centroid of each possible symbol on each of the polarization subchannels. After training, the receiver was switched to pilot-aided (PA) operation. In this mode, information from periodic pilot symbols was used in combination with channel statistics to update the adaptive equalizer and carrier phase estimate.

For all cases, the received signal was initially de-skewed and normalized on a per-quadrature basis to correct for imperfections in the receiver front-end. After this, the input signal was demultiplexed into constituent subcarriers, and each subcarrier resampled to two samples per symbol. A digital anti-aliasing filter was used before resampling, in order to prevent aliasing induced crosstalk. The filter was wide enough to avoid in-band distortion of the received signal subcarriers.

IV. Receiver Training DSP Algorithms

For each subchannel, initial blind estimation of intradyne-frequency (IF) is performed. Coarse estimation of the timing phase is performed with a dual-polarization (DP) constant modulus algorithm (CMA) equalizer, with least-mean square (LMS) tap updating. The output symbols from this equalizer are then raised to the power of 4, and the resultant spectrum is used to determine the IF for each subcarrier.

Initial processing in training mode was performed using a blind (DP-CMA) with LMS updating, followed by Viterbi & Viterbi 4th power carrier phase estimation [18]. This enabled sufficiently accurate signal recovery to perform synchronization of the received signal with the training sequence.

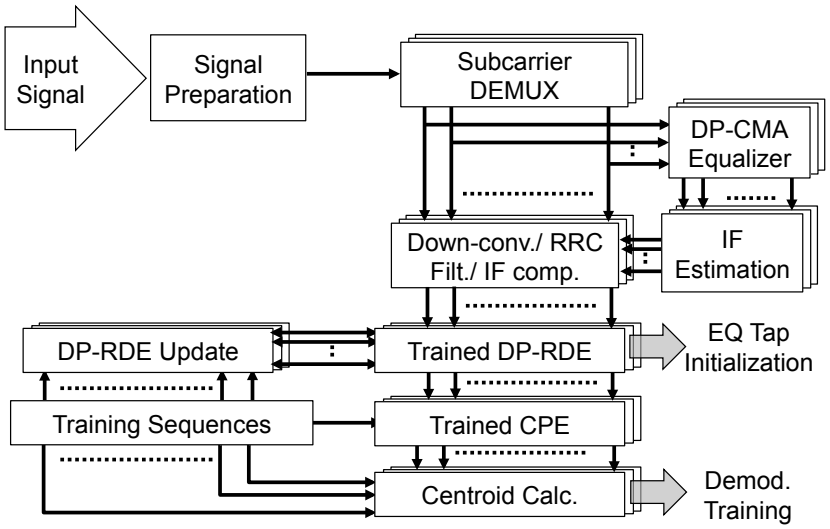

Fig. 4. Schematic of receiver operation in training mode.

A. Equalizer training

For each subchannel, a DP radius-directed equalizer (RDE) with LMS updating was used to equalize polarization rotations and filtering impairments, and to recover the timing phase. The output v of the equalizer at time k, for polarizations x and y is given by

$$v_x(k) = \mathbf{h}_{xx}^H \mathbf{u}_x + \mathbf{h}_{xy}^H \mathbf{u}_y, \tag{1}$$

$$v_y(k) = \mathbf{h}_{yx}^H \mathbf{u}_x + \mathbf{h}_{yy}^H \mathbf{u}_y, \tag{2}$$

where $\mathbf{u}_x$ and $\mathbf{u}_y$ are the input (column) vectors for the x and y polarizations, H denotes the Hermitian transpose, and the four FIR filter vectors are $\mathbf{h}_{xx}$, $\mathbf{h}_{xy}$, $\mathbf{h}_{yx}$ and $\mathbf{h}_{yy}$.

The equalizer was trained based on the radius of the symbols in the training sequence. The trained equalizer error terms were calculated with the following equations:

$$e_x(k) = |T_x(k)|^2 - |v_x(k)|^2, \quad e_y(k) = |T_y(k)|^2 - |v_y(k)|^2, \tag{3}$$

where $T_x(k)$ and $T_y(k)$ are the training symbols at time k on the x and y polarizations, respectively. This leads to the LMS update for the filters given by:

$$\mathbf{h_{xx}}' = \mathbf{h_{xx}} + \mu e_x(k) \mathbf{u_x} v_x^*(k), \tag{4}$$

$$\mathbf{h_{xy}}' = \mathbf{h_{xy}} + \mu e_x(k) \mathbf{u_y} v_x^*(k), \tag{5}$$

$$\mathbf{h_{yx}}' = \mathbf{h_{yx}} + \mu e_y(k) \mathbf{u_x} v_y^*(k), \tag{6}$$

$$\mathbf{h_{yy}}' = \mathbf{h_{yy}} + \mu e_y(k) \mathbf{u_y} v_y^*(k), \tag{7}$$

where the conjugation operator is denoted by *.

By using a trained equalizer adapted only on the radius of the received signals, we were able to attain excellent equalization of the signal with unconstrained phase. This enabled us to have an equalization structure which could adapt slowly in response to the slowly varying polarization channel, while phase tracking could be performed with a significantly higher rate of tracking.

B. Carrier phase estimation training

Carrier phase estimation (CPE) was performed using a data-aided feedforward algorithm, somewhat similar to the non-data-aided algorithm proposed in [19]. A phase estimate ϕ is calculated at time k by multiplying the Hermitian transpose of an input vector $\mathbf{v}$ with the training symbol vector $\mathbf{T}$, and taking the complex argument:

$$\phi(k) = \arg(\mathbf{v}^H \mathbf{T}). \tag{8}$$

We note that this phase estimate does not require unwrapping, as it is already on the interval $(-\pi, \pi]$. The input signal v is then corrected for phase at instant k, to produce a phase corrected output r according to:

$$r(k) = v(k) e^{j\phi(k)}. \tag{9}$$

C. Centroid calculation

After correcting for the phase noise on the training sequence, we were able to calculate the centroid of each of the 64 constellation points, and the SNR for each of the 22 polarization subchannels. For each symbol s in the set of symbols S, a new symbol s' was calculated as the complex mean of the received training symbols r which correspond to transmitted training symbols t being equal to s as follows:

$$s' = \mathbb{E}(r|t = s), \quad \forall s \in S, \tag{10}$$

where $\mathbb{E}$ denotes expectation. The new set of distorted symbols S' were subsequently used in the pilot-aided CPE, and the calculation of bit log-likelihood ratios (LLRs) [20].

V. Pilot-aided DSP algorithms

After training had led to a well converged equalizer, with accurately calculated IF offsets and constellation centroids, the receiver was switched to pilot-aided operation, with a 1% pilot-insertion ratio (PIR). A schematic of the pilot-aided receiver operation is shown in Fig. 5. The frequency subchannels were prepared as before, with IF correction and matched RRC filtering being performed before any pilot-aided processing.

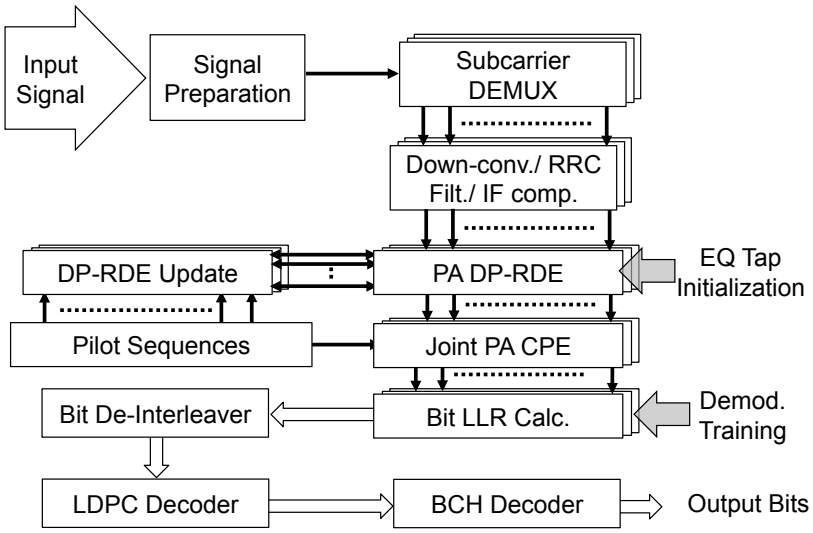

Fig. 5. Schematic of receiver operation in pilot-aided mode. Initial equalizer tap values and signal constellation centroids are learned during the receiver training period.

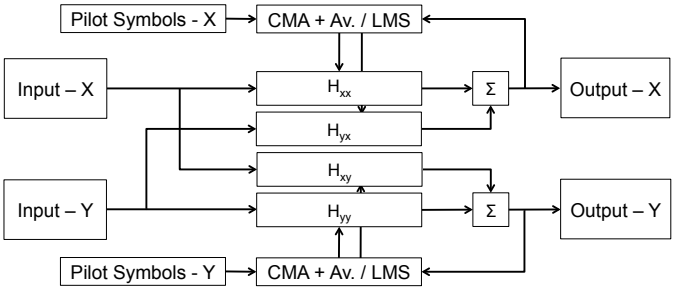

Fig. 6. Schematic of pilot-aided CMA equalizer.

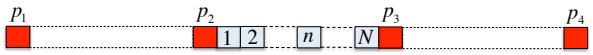

Fig. 7. Illustration of multi-pilot estimation with $2L = 4$ pilots.

Adaptation of the equalizer was performed every 10 pilot symbols, by averaging the error over a block of 10 pilots. This sub-rate adaptation enabled us to further reduce the influence of tap noise while operating with a step-size parameter of $\mu = 10^{-4}$.

A. Pilot-aided equalization

The equalizer taps previously calculated during training mode were used as the initial state of the pilot-aided equalizers. A pilot-aided DP-CMA (PA-DP-CMA) algorithm was used for each frequency subcarrier, with the error calculation being performed only for the pilot symbols (rather than every symbol during training mode). A schematic of this equalizer can be seen in Fig. 6. We note again that this equalizer structure is – like the conventional DP-RDE algorithm – immune to the effects of phase noise [21]. However, unlike the DP-RDE, the PA-DP-CMA algorithm is immune to the effects of noise artifacts introduced by incorrect decisions in the equalizer.

The pilot-aided equalizer was adapted according to the following equations:

$$e_x(k) = \frac{1}{10}\sum_{i=0}^{9}\left(|P_x(k-100i)|^2 - |v_x(k-100i)|^2\right), \quad (11)$$

$$e_y(k) = \frac{1}{10}\sum_{i=0}^{9}\left(|P_y(k-100i)|^2 - |v_y(k-100i)|^2\right), \quad (12)$$

where $P_x(k)$ and $P_y(k)$ are pilot symbols at time k on the x and y polarizations, respectively. This leads to the LMS update for the filters given by (4)–(7).

B. Pilot-aided carrier phase estimation

First, we describe in detail the multi-pilot-aided CPE algorithm which we have previously proposed [22] and experimentally demonstrated [23]. Then, we generalize it for joint carrier phase estimation of multiple channels when phase evolution is correlated over several wavelength subchannels.

We assume that N information symbols are transmitted in a block and that each block starts with a pilot symbol. To estimate phase of a symbol transmitted during the k^{th} signaling interval, we use L_1 pilots preceding and L_2 pilots following the considered symbol, and without loss of generality assume $L_1 = L_2 = L$. Therefore, phases of information symbols belonging to the same block are estimated using the same set of pilots $P = \{p(1), \ldots, p(L), p(L+1), \ldots, p(2L)\}$. Note that a single pilot might belong to more than one set of pilots. Also note that phases of information symbols from different blocks are estimated with the aid of different sets of pilots. For example, phases of the symbols between pilots $p(2)$ and $p(3)$ in Fig. 7 are estimated using pilots $p(1), p(2), p(3)$ and $p(4)$.

1) Phase noise model: Assuming all signal impairments but phase and additive noise have been compensated, a sample of the received signal at discrete time k, $v(k)$, is related to

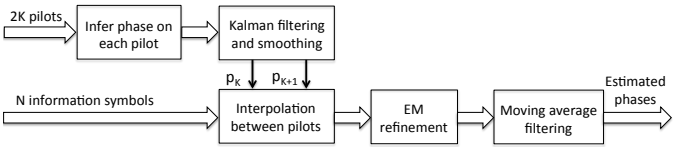

Fig. 8. Processing steps in our pilot-aided CPE algorithm.

the symbol transmitted in the corresponding signaling interval, $s(k)$, as

$$v(k) = s(k)e^{j\theta(k)} + n(k), \tag{13}$$

where $\theta(k)$ and $n(k)$ are, respectively, the samples of a real phase noise and complex circularly symmetric additive white Gaussian noise (AWGN). That is, $n(k) \sim \mathcal{CN}(0, \sigma_n^2)$, while $\theta(k)$ is modeled as a Wiener process, i.e.,

$$\theta(k) - \theta(k-1) \sim \mathcal{N}(0, \sigma_\rho^2), \quad \sigma_\rho^2 = 2\pi\Delta\nu\tau_s, \tag{14}$$

where $\Delta\nu$ is the combined linewidth of transmitter's and receiver's lasers and τ_s is the symbol period. Since the consecutive pilots $p(\zeta)$ and $p(\zeta+1)$ are separated by $N+1$ signaling intervals (i.e., by N information symbols), we note using (14) that

$$\theta_{p(\zeta+1)} - \theta_{p(\zeta)} \sim \mathcal{N}(0, (N+1)\sigma_\rho^2), \tag{15}$$

where $\zeta = 1, \ldots, 2L-1$.

We frame the phase estimation problem by means of the statistical inference with the goal to compute/approximate the probability distribution of unknown phase $\theta(k)$, conditioned on the transmitted and received signals at pilot locations. That is, the proposed algorithm approximates $\Pr(\theta(k)|v(k), s_{p(\zeta)}, v_{p(\zeta)}, \zeta = 1, \ldots, 2L), k = 1, \ldots, N$, which is carried out through the steps outlined in Fig. 8.

2) Inference of Pilot Phases: Initially, the algorithm approximates the posterior distribution $\Pr(\theta_{p(\zeta)}|s_{p(\zeta)}, v_{p(\zeta)})$ of an unknown phase of pilot location $p(\zeta)$, given the corresponding transmitted pilot symbol $s_{p(\zeta)}$ and received signal $v_{p(\zeta)}$. This posterior can be, in principle, evaluated using the Bayes' rule and model (13). However, this approach does not yield a closed form expression for the posterior distribution and we thus approximate it. Using the Laplace approximation [24], the pilot symbol phases are approximated (after few steps of derivations which are omitted here) as

$$\theta_{p(\zeta)}|s_{p(\zeta)}, v_{p(\zeta)} \sim \mathcal{N}(\mu_{p(\zeta)}, \sigma_{p(\zeta)}^2), \tag{16}$$

where

$$\mu_{p(\zeta)} = \arg\{v_{p(\zeta)}s_{p(\zeta)}^*\}, \tag{17}$$

and

$$\sigma_{p(\zeta)}^2 = \frac{\sigma_n^2}{2|s_{p(\zeta)}v_{p(\zeta)}|}. \tag{18}$$

Note that the above computations are performed for each pilot in parallel.

After this initial step, we evaluated the posterior $p(\theta_{p(k)}|s_{p(\zeta)}, v_{p(\zeta)}, \zeta = 1, \ldots, 2L)$, of the pilot $p(k)$'s ($k = 1, \ldots, 2L$) phase, conditioned on the knowledge of the transmitted symbols and received signals corresponding to all pilots from the set P. In doing so, we use the Kalman filtering framework. Towards that end, we need to specify the underlying linear dynamical model and observation model. The linear dynamical model is simply the Wiener phase noise model in (14). On the other hand, the observation model is constructed as

$$\psi_{p(\zeta)} = \theta_{p(\zeta)} + n_{p(\zeta)}, \tag{19}$$

where

$$\psi_{p(\zeta)} = \mu_{p(\zeta)}, \tag{20}$$

and

$$n_{p(\zeta)} \sim \mathcal{N}(0, \sigma_{p(\zeta)}^2), \tag{21}$$

where $\mu_{p(\zeta)}$ and $\sigma_{p(\zeta)}^2$ are as evaluated in (17) and (18). Intuitively, $\psi_{p(\zeta)}$ is a noisy "observation" of an unknown phase, where $n_{p(\zeta)}$ is the observation noise.

Applying the Kalman smoother with linear dynamical (14) and observation model (19) yields

$$\begin{aligned}&\theta_{p(\zeta)}|s_{p(1)}, v_{p(1)}, \ldots, s_{p(2L)}, v_{p(2L)} \\ &\sim \mathcal{N}(\nu_{p(\zeta)}, \tilde{\sigma}_{p(\zeta)}^2), \quad \zeta = 1, \ldots, 2L,\end{aligned} \tag{22}$$

where mean $\nu_{p(\zeta)}$ and variance $\tilde{\sigma}_{p(\zeta)}^2$ are evaluated using the forward and backward pass through the model.

In fact, 22 is the only step in our method which requires sequential processing. To speed up this processing step, we can reduce the number of pilots in the set P. In fact, our study shows that for 64-QAM and for relevant phase noise regimes, increasing the number of pilots $2L$ beyond 4 provides only negligible performance gains. Also, this step requires a backward pass which stops at pilot $p(L+1)$, which saves us from doing L steps in the backward pass (refer to (24)).

Alternatively, the processing in this step could also be done in parallel if the computational resources allow for performing inversion of a matrix of size $2L$ on each pilot. This is also a reasonable approach since $2L = 4$ already brings us to the edge of possible performance improvements for the systems of our interest.

3) Estimation of Information Symbol Phases: In this stage, initial estimates of the information symbol phases are obtained by interpolating between pilots symbol phases, estimated in the previous stage. The initial phase estimates are then refined by means of the expectation maximization (EM) method [24].

Recalling that the information symbols are between pilots $p(L)$ and $p(L+1)$ and using Wiener process model for phase noise (14), it is shown that the posterior $\Pr(\theta(k)|s_{p(\zeta)}, v_{p(\zeta)}, \zeta = 1, \ldots, 2L)$ is Gaussian distributed with mean and variance dependent upon means and variances of Gaussian posteriors corresponding to the pilots $p(L)$ and $p(L+1)$.

More precisely, it can be shown that

$$\theta(k)|s_{p(1)}, v_{p(1)}, \ldots, s_{p(2L)}, v_{p(2L)} \sim \mathcal{N}(\mu_k, \sigma_k^2), \tag{23}$$

where

$$\mu(k) = \frac{(N+1-k)\sigma_\rho^2\tilde{\mu}_{p(L)} + (k\sigma_\rho^2 + \tilde{\sigma}_{p(L)}^2)\nu_{p(L+1)}}{(N+1)\sigma_\rho^2 + \tilde{\sigma}_{p(L)}^2}, \tag{24}$$

where $\tilde{\mu}_{p(L)}$ is the mean of the resulting distribution obtained from Kalman's forward pass corresponding to pilot $p(L)$,

while $\nu_{p(L+1)}$ is the mean of the resulting distribution obtained from the Kalman's backward pass corresponding to pilot $p(L+1)$. As mentioned in the previous part, the backward pass ends on pilot $p(L+1)$. Note that (24) is performed in parallel on all information symbols within a block.

The estimates of the information symbol phases in (24) are then refined by employing the EM algorithm. Note that the application of the EM algorithm is well suited after reasonably accurate phase estimates have been obtained. Namely, due to a non-convex nature of the underlying optimization function, the EM algorithm converges to a local stationary point closest to the initial point. Therefore, the EM algorithm needs to be initialized with a phase estimate that is already reasonably close to the true phase to yield better phase estimate.

A separate EM procedure refines the phase estimate of each information symbol in parallel. In the following, we present the computations involved and skip the derivation details. The EM routine on symbol $s(k)$ is initialized with $\hat{\theta}_{(0)}(k) = \mu(k)$, where $\mu(k)$ is the phase estimate obtained from (24). The q-th iteration starts with evaluating the likelihood of symbol $s(k)$ given the received signal $v(k)$ and phase estimate $\hat{\theta}_{(q-1)}(k)$, obtained from the iteration $q-1$. This likelihood is up to the normalization constant given by

$$\begin{aligned} & \Pr(s(k)=a|v(k);\hat{\theta}_{(q-1)}(k)) \\ \propto\ & \Pr(v(k)|s(k)=a;\hat{\theta}_{(q-1)}(k))\Pr(s(k)=a;\hat{\theta}_{(q-1)}(k)) \\ \propto\ & \exp\left(-\frac{1}{\sigma_n^2}\left|v(k)-ae^{j\hat{\theta}_{(q-1)}(k)}\right|^2\right), \end{aligned} \tag{25}$$

where $s(k)$ takes values from the transmitted constellation, i.e., $a \in S$, and without loss of generality we assume that transmitted symbols are equally likely. The symbol likelihoods are then used to update the phase estimate as

$$\hat{\theta}_{(q)}(k) = \arg\left(v(k)\sum_{a\in S} a^* \Pr(s(k)=a|v(k);\hat{\theta}_{(q-1)}(k))\right). \tag{26}$$

The EM algorithm is performed until a termination condition is satisfied, e.g., until a predefined number of iterations $Q_{\max}$. To reduce the computational complexity, the number of iterations $Q_{\max}$ can be kept to a small value. Our study shows that the algorithm converges after 2 iterations and no improvement is made by using more than 2 iterations. Additionally, the complexity burden arising from computing the symbol likelihoods for high order modulation formats (such as 64-QAM or 256-QAM) can be alleviated by taking into account only the constellation points close to the initial soft symbol estimate obtained by applying initial phase estimate (24) onto corresponding received signal $v(k)$.

The EM procedures are performed separately on information symbols (and thus in parallel) such that the correlation structure of phase variations across symbols is not exploited. We point out that in principle it is possible to formulate the EM procedure which takes into account the statistics of phase variations. However, the phase estimates in such a procedure are not given in closed forms. More importantly, such a procedure does not admit parallel implementation and is therefore not practical.

To overcome the shortcoming of not taking into account the statistics of phase variations in the EM procedures, the proposed method filters the EM phase estimates $\hat{\theta}_{(Q_{\max})}(k)$ by applying a moving average filter of length $2L_F+1$. That is, the final phase estimate is computed as

$$\hat{\theta}(k) = \frac{1}{2L_F+1}\sum_{i=k-L_F}^{k+L_F} \hat{\theta}_{(Q_{\max})}(i), \tag{27}$$

where $\hat{\theta}_{(Q_{\max})}$ is the phase estimate obtained as a result of the EM step.

The described method outputs the phase estimates of the information symbols. In addition, we can apply these phase estimates on the received symbols and output soft and/or hard estimates of the transmitted symbols.

4) Generalization to Multiple Channels: In this part, we generalize the described method for CPE of a single channel to the case where phase noise variations across multiple channels (e.g., x and y polarizations of a single wavelength channel or all x and y polarizations of channels in a superchannel) are correlated.

We denote with C the number of channels in a multi-channel system. The signal received in channel c at time k is modeled as

$$v_c(k) = s_c(k)e^{j\theta_c(k)} + n_c(k), \quad c = 1,2,\ldots,C, \tag{28}$$

where $s_c(k)$ is the transmitted symbol, $\theta_c(k)$ is phase and $n_c(k)$ is noise, all corresponding to channel c at discrete time k. The noise is modeled as $n_c(k) \sim \mathcal{CN}(0,\sigma^2_{n(c)})$. Note that the variance of the additive noise is not necessarily the same in different channels.

Each channel transmits a block of information symbols, preceded by a pilot symbol. The phase estimation of information symbols within a block is aided with L pilots preceding and L pilots following the block. In general, the number of pilots used on each side and in each channel can be different.

Our phase estimation method proceeds in a similar way as for a single channel case. That is, the means $\mu_{p(c,\zeta)}$ and variances $\sigma^2_{p(c,\zeta)}$ of approximating Gaussian posteriors of pilot symbol phases are evaluated for each pilot in each channel by using (17) and (18). The initial pilot phase estimates are processed using the Kalman filtering framework. In comparison to a single channel case, the phases of pilots across channels and polarizations appearing at the same discrete time are collected into a state vector $\boldsymbol{\theta}_{p(\zeta)} = \begin{bmatrix} \theta_{p(1,\zeta)} & \ldots & \theta_{p(2C,\zeta)} \end{bmatrix}^T$. We assume the linear dynamical model for state vector is given by

$$\boldsymbol{\theta}_{p(\zeta+1)} - \boldsymbol{\theta}_{p(\zeta)} \sim \mathcal{N}(\mathbf{0},(N+1)\sigma_\rho^2\mathbf{C}), \zeta = 1,\ldots,2L-1, \tag{29}$$

where $\mathbf{C}$ is a matrix of correlation coefficients between phase noise jumps across channels and polarizations. This correlation matrix is predefined or estimated in the training mode. The observation model is similarly to a single channel case given by

$$\boldsymbol{\psi}_{p(\zeta)} = \boldsymbol{\theta}_{p(\zeta)} + \mathbf{n}_{p(\zeta)}, \quad \zeta = 1,\ldots,2L, \tag{30}$$

where the observed vector $\boldsymbol{\psi}_{p(\zeta)} = \boldsymbol{\mu}_{p(\zeta)}$ and $\mathbf{n}_{p(\zeta)} \sim \mathcal{N}(\mathbf{0},\boldsymbol{\Sigma}_{p(\zeta)})$, where $\boldsymbol{\Sigma}_{p(\zeta)} = \mathrm{diag}(\sigma^2_{p(1,\zeta)},\ldots,\sigma^2_{p(2C,\zeta)})$.

Given the linear dynamical and observation model, the proposed method processes the initial pilot phase estimates via full forward pass of Kalman filtering and backward pass of Kalman smoothing up to pilot $p(L+1)$. The outputs of this processing stage are the mean vector $\tilde{\boldsymbol{\mu}}_{p(L)}$ and covariance matrix $\tilde{\boldsymbol{\Sigma}}_{p(L)}$ corresponding to the pilot $p(L)$, obtained from the forward pass, as well as the mean vector $\boldsymbol{\nu}_{p(L+1)}$, corresponding to the pilot $p(L+1)$, resulting from the backward pass.

Note that each step of sequential processing required in the Kalman stage performs matrix inversion, where the matrix size is equal to $2C$, i.e., all polarizations and channels. To alleviate the computational burden, one may reduce the number of pilots $2L$ aiding phase estimation. Our study with 64-QAM shows that using more than 4 pilots (2 on each side) provides no further gains.

The second stage of the proposed method first delivers initial estimates of information symbol phases, obtained from interpolating between phases corresponding to pilots $p(L)$ and $p(L+1)$, inferred in the previous stage. Conceptually, one can interpolate between two Gaussian vectors (inferred phases across channels at locations $p(L)$ and $p(L+1)$). However, this would necessitate computing N matrix inversions (one for each information symbol in a block). To alleviate this shortcoming, we perform interpolation between phases in each channel separately. Therefore, the initial phase estimate of a symbol k in channel c is computed by

$$\mu(c,k) = \frac{(N+1-k)\sigma_\rho^2 \tilde{\mu}_{p(c,L)} + (k\sigma_\rho^2 + \tilde{\sigma}^2_{p(c,L)})\nu_{p(c,L+1)}}{(N+1)\sigma_\rho^2 + \tilde{\sigma}^2_{p(c,L)}}, \tag{31}$$

where $\tilde{\mu}_{p(c,L)}$ and $\nu_{p(c,L+1)}$ are the c-th entries in respectively $\tilde{\boldsymbol{\mu}}_{p(L)}$ and $\boldsymbol{\nu}_{p(L+1)}$, while $\tilde{\sigma}^2_{p(r,L)}$ is the c-th diagonal element of $\tilde{\boldsymbol{\Sigma}}_{p(L)}$.

The initial phase estimates of information symbols are then refined using the EM procedure as previously detailed. The EM procedure is applied to each information symbol in each channel in parallel. The details are the same as for a single channel case. Note that the correlations between phases in different channels are not taken into account by running separate EM procedures. Conceptually, the EM procedures can be devised so as to account for these correlations. However, this would require more complicated routines for updating phase estimates. More specifically, a vector of phase estimates across channels at some discrete time would be updated as a vector which minimizes the corresponding objective function and is not given in a closed form.

The final phase estimates are obtained by filtering the EM phase estimates with the moving average filter applied in each channel separately. The outputs from the moving average filter are the final phase estimates. They can be applied to the received signal to yield soft and/or hard estimates of the transmitted symbols.

C. Forward Error Correction Coding

After CPE was performed, we calculated bit-wise LLRs with the modified signal set calculated in (10). As we previously noted, this method of LLR calculation allowed us to mitigate the impact of imperfect modulation [20]. We then de-interleaved the signal over all subchannels, such that each codeword contained approximately equal proportions of each of the bit-positions and subchannels. This enables the system performance to be determined by the average generalized mutual information (GMI), rather than the worst subchannel or bit position [25]. Following this, we normalized the bit LLRs such that each bit was detected as though '0' was transmitted. This enabled us to test a variety of LDPC codes, by decoding the all zero codeword, which exists in all linear codes. Although we manipulated the LLR signs, no LLR values were changed, and the information content of the signal was preserved.

We used a check-concentrated irregular low-density parity-check (LDPC) (105600,82368) code [26] with rate 0.78 for the inner code. LDPC decoding was performed with 60 iterations of the sum-product algorithm, and flooding scheduling. While this is a somewhat large number of iterations for an LDPC decoder (compared with, for example, 16 iterations used in [27]), we do not consider this to be of-itself a condition for high decoder complexity. Decoder complexity and latency is discussed in detail in our work presented in [28], wherein we analyze the effects of degree distribution, iteration count, and other topics which are beyond the scope of this work.

We assumed the use of an outer Bose–Chaudhuri–Hocquenghem (BCH) (30832,30592) code (rate 0.9922) [29] with minimum Hamming distance of 33. We have calculated a union (upper) bound of 10^{-15} on the outer decoder output bit error rate (BER) given an input BER of 5×10^{-5}. Therefore, the input BER threshold for this outer code is at or above an input BER of 5×10^{-5}. Alternatively, a BER of 5×10^{-5} or less at the output of the LDPC decoder can be successfully decoded to 10^{-15} or lower when the previously described outer BCH code is used.

VI. Results

The results presented in this section describe successful measurement of a 1 Tb/s superchannel back-to-back, and without optical noise loading.

By training all 11 of the 2×2 DP-RDE equalizers independently, we are able to achieve equalization with very low DSP penalty. We note from the taps for the central subchannel (shown in Fig. 9), that the impulse response of the channel is longer than may be expected, and 301 taps were required for good performance. We attribute this to filtering effects from the receiver photodiodes and ADCs, which are operating at extremely high frequencies (more than 50 GHz).

We note from the experimental measurement shown in Fig. 10, that the output phases are – as expected – highly correlated between polarization subchannels. We also note that there are varying offsets between these subchannels which remain approximately constant. This is due to the difference in optical path lengths seen by each subchannel, including differences introduced by polarization and frequency sensitive components.

By examining the BER after the CPE has been performed, we noted a wide variation in performance from 8×10^{-3} to

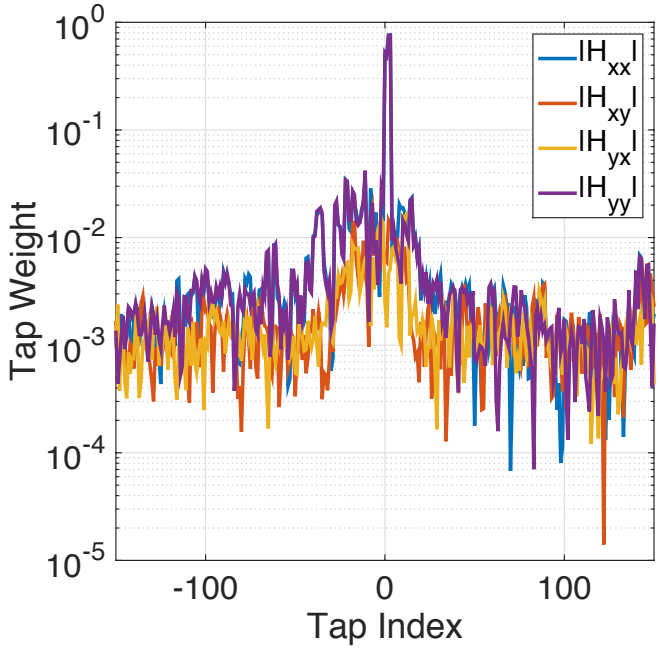

Fig. 9. Absolute value of the converged equalizer taps for the central subchannel after the training period. Note the long response time of the system, necessitating a long equalizer of 301 taps.

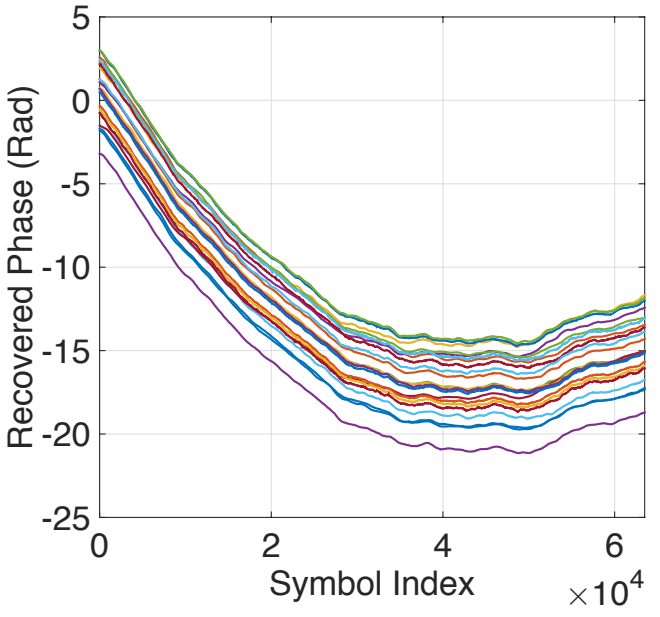

Fig. 10. Estimated carrier phases, from multi-channel pilot-aided estimation algorithm. Note the high degree of similarity between the estimated phases.

1.4×10^{-1} over the different frequency subchannels (although performance between different polarizations on the same frequency was approximately equal), in Fig. 11. We speculate that this variation in performance may be due to imperfect balancing of the optical comb, in combination with the high loss in the optical comb equalizer and deinterleaver. The combination of these effects may have caused variation in the noise figure of the transmitter EDFAs over the range of frequencies in the

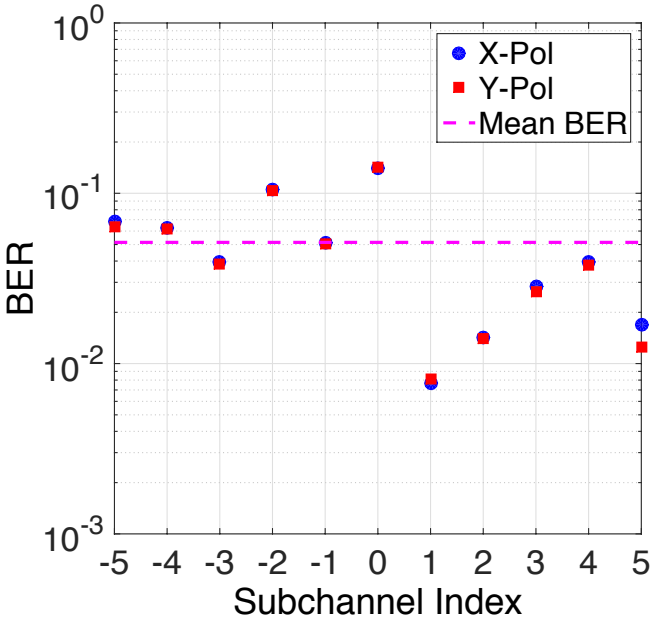

Fig. 11. Measured bit error rate for each polarization of the 11 frequency subchannels. Note the wide variation in performance for different frequencies.

superchannel. While it is not possible to determine the origin of a source of additive noise from post-processing alone, we may make some reasonable deductions. Due to the uneven nature of both the BER and measured subchannel SNRs, and the accurate and highly correlated recovered carrier phase, we believe that the variation in performance is unlikely to be due to analog electronic or DSP subsystems, while the variation in optical powers in the optical comb after deinterleaving and equalization seems to be a likely culprit for this distortion.

Despite this variation in the effective SNR over the different subchannels, we note that our pilot-aided CPE algorithm is sufficiently robust that the phases of all subchannels are recovered without cycle slips or significant failures in estimation. While a detailed comparison of pilot-aided and non-pilot-aided CPE algorithms is beyond the scope of this work, we would like to direct the interested reader to our previous work on this topic in [22] and [23].

The convergence of the LDPC decoder is shown in Fig. 12. We note that despite the large variation in pre-FEC BER, convergence is still possible, and the sum-product decoder has achieved an output below the threshold of the outer code in 47 iterations, while after 55 iterations, no bit errors are detected in any of the 74 codewords detected ($\sim$7.8 million bits).

The union bound on input BER for a given output BER is shown in Fig. 13. By calculating a lower bound on the input BER for a given output BER of 10^{-15}, we have determined that the threshold for this code is at or above 5×10^{-5}.

VII. Conclusions

We have described in detail the design of a digital coherent receiver that is capable of detecting a 1 Tb/s superchannel. The optical transmitter and receiver used in the experiment were described in detail. Receiver training was described in

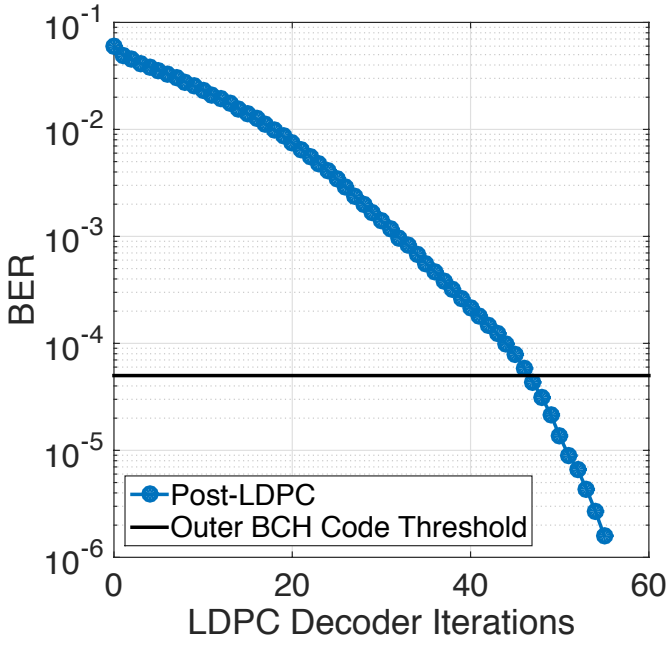

Fig. 12. Convergence of the LDPC decoder (sum-product algorithm) for experimental results. Mean BER is shown over 74 codewords (∼7.8 million bits).

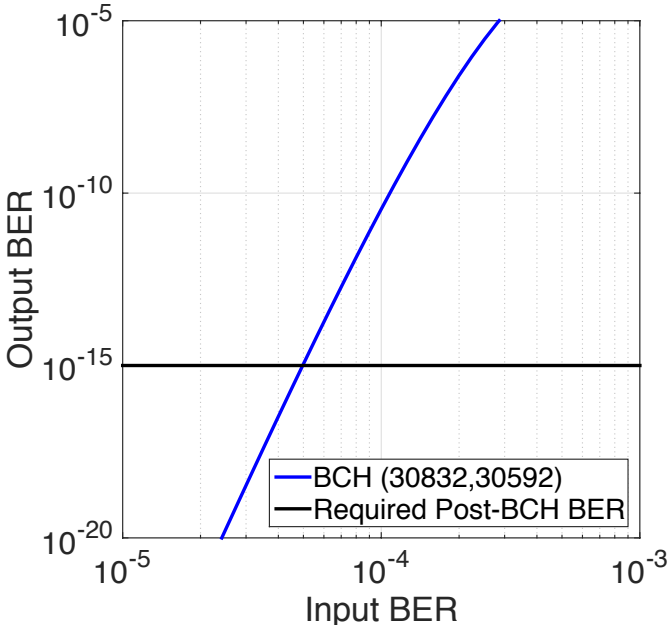

Fig. 13. Union (lower) bound on the input BER for a given output BER. BER threshold of this code is inferred to be 5×10^{-5} or higher.

detail, with the aim of learning the equalizer taps, the SNR of each subchannel, and the set of constellation centroids for each subchannel. We then described in detail the algorithms used for pilot-aided receiver operation. A pilot-aided DP-CMA algorithm was then described for accurate per-subchannel equalization. An extension of our previously described pilot-aided CPE was described to jointly estimate carrier phase over several subcarriers with shared transmitter and receiver lasers. We then described the forward error correction scheme proposed for this system, with an inner rate 0.78 LDPC code and an outer BCH code which can correct an input BER of 5×10^{-5} to an output BER of 10^{-15} or lower. We note that all algorithms used in this work are of moderate complexity, and suitable for parallel implementation in hardware.

Results were then given, demonstrating operation at a net data-rate of more than 1 Tb/s with a single digital coherent receiver. A Nyquist-spaced coherent superchannel, consisting of 11×10 GBd DP-64QAM (gross bit rate of 1.32 Tb/s) was detected with an ultra-high bandwidth receiver. Pilot-aided DSP algorithms of moderate complexity and suitable for hardware implementation were used, enabling robust performance over varying subchannel SNRs with 1% pilot symbols. An inner LDPC code and an outer BCH code were used, with combined overhead of 29.2%, resulting in a net bit-rate of 1.012 Tb/s.

REFERENCES

[1] G. Raybon et al., "All-ETDM 107-Gbaud PDM-16QAM (856-Gb/s) transmitter and coherent receiver," in *Proc. Euro. Conf. on Optical Commun.*, London, UK, Sept. 2013, PD2D3.

[2] S. Beppu, K. Kasai, M. Yoshida, and M. Nakazawa, "2048 QAM (66 Gbit/s) single-carrier coherent optical transmission over 150 km with a potential SE of 15.3 bit/s/Hz," in *Proc. Opt. Fiber Commun. Conf.*, San Francisco, CA, USA, Mar. 2014, W1A6.

[3] C. Zhang, Y. Mori, K. Igarashi, K. Katoh, and K. Kikuchi, "Demodulation of 1.28-Tbit/s polarization-multiplexed 16-QAM signals on a single carrier with digital coherent receiver," in *Proc. Opt. Fiber Commun. Conf.*, San Diego, CA, USA, Mar. 2009, OTuG3.

[4] J. K. Fischer et al., "High-speed digital coherent receiver based on parallel optical sampling," J. Lightw. Technol., vol. 29, no. 4, pp. 378–385, 2011.

[5] N. K. Fontaine et al., "Fiber nonlinearity compensation by digital backpropagation of an entire 1.2-Tb/s superchannel using a full-field spectrally-sliced receiver," in *Proc. Euro. Conf. on Optical Commun.*, London, UK, Sept. 2013, Mo3D5.

[6] R. Rios-Müller et al., "1-terabit/s net data-rate transceiver based on single-carrier Nyquist-shaped 124 GBaud PDM-32QAM," in *Proc. Opt. Fiber Commun. Conf.*, Los Angeles, CA, USA, Mar. 2015, Th5B1.

[7] T. Richter et al., "Distributed 1-Tb/s all-optical aggregation capacity in 125-GHz optical bandwidth by frequency conversion in fiber," in *Proc. Euro. Conf. on Optical Commun.*, London, UK, Sept. 2013, PDP.2.5.

[8] D. S. Millar et al., "Detection of a 1 Tb/s superchannel with a single coherent receiver," in *Proc. Euro. Conf. on Optical Commun.*, Valencia, ES, Sept. 2015, Mo.3.3.1.

[9] Z. Zhang et al., "Coherent transceiver operating at 61-Gbaud/s," Optics Express, vol. 23, no. 15, pp.18988–18995, 2015.

[10] (2015, Jul.) "Technology Options for 400G Implementation," [Online]. Available: http://www.oiforum.com/wp-content/uploads/OIF-Tech-Options-400G-01.0.pdf

[11] (2015, Oct.) Keysight M8196A Data Sheet, [Online]. Available: http://literature.cdn.keysight.com/litweb/pdf/5992-0971EN.pdf?id=2631835

[12] (2015, Oct.) Teledyne LeCroy Labmaster 10Zi Data Sheet, [Online]. Available: http://cdn.teledynelecroy.com/files/pdf/labmaster-10zi-a-datasheet.pdf

[13] G. Bosco, V. Curri, A. Carena, P. Poggiolini, and F. Forghieri, "On the performance of Nyquist-WDM terabit superchannels based on PM-BPSK, PM-QPSK, PM-8QAM or PM-16QAM subcarriers," J. Lightw. Technol., vol. 29, no. 1, pp. 53–61, 2011.

[14] H. Mardoyan et al., "Transmission of single-carrier Nyquist-shaped 1-Tb/s line-rate signal over 3,000 km," in *Proc. Opt. Fiber Commun. Conf.*, Los Angeles, CA, USA, Mar. 2015, W3G2.

[15] G. Raybon et al., "160-Gbaud coherent receiver based on 100-GHz bandwidth, 240-GS/s analog-to-digital conversion," in *Proc. Opt. Fiber Commun. Conf.*, Los Angeles, CA, USA, Mar. 2015, M2G1.

[16] R. Maher et al., "Spectrally shaped DP-16QAM super-channel transmission with multi-channel digital back-propagation," Nat. Sci. Rep., vol. 5, 2015, pp. 8214, 2015.

[17] D. S. Millar et al., "Transceiver-limited high spectral efficiency Nyquist-WDM systems," in *Proc. Opt. Fiber Commun. Conf.*, Los Angeles, CA, USA, Mar. 2015, Th2A13.

[18] S. J. Savory, "Digital coherent optical receivers: Algorithms and subsystems," IEEE J. Sel. Topics. Quantum Electron., vol. 16, no. 5, pp. 1164–1179, 2010.
[19] S. Makovejs et al., "Characterization of long-haul 112Gbit/s PDM-QAM-16 transmission with and without digital nonlinearity compensation," Optics Express, vol. 18, no. 12, pp. 12939–12947, 2011.
[20] T. Koike-Akino, D. S. Millar, K. Kojima, and K. Parsons, "Phase noise-robust LLR calculation with linear/bilinear transform for LDPC-coded coherent communications," in *Proc. Conf. on Lasers and Electro-Optics*, San Jose, CA, USA, June 2015, SW1M.3.
[21] I. Fatadin, D. Ives, and S. J. Savory, "Blind equalization and carrier phase recovery in a 16-QAM optical coherent system," J. Lightw. Technol., vol. 27, no. 15, pp. 3042–3049, 2009.
[22] M. Pajovic, D. S. Millar, T. Koike-Akino, K. Kojima, V. Arlunno, and K. Parsons, "Multi-pilot aided carrier phase estimation for single carrier coherent systems," in *Proc. Sig. Process. Photon. Commun.*, Boston, MA, USA, July 2015, SpT4D.4.
[23] M. Pajovic et al., "Experimental demonstration of multi-pilot aided carrier phase estimation for DP-64QAM and DP-256QAM," in *Proc. Euro. Conf. on Optical Commun.*, Valencia, ES, Sept. 2015, Mo.4.3.3.
[24] C. M. Bishop, "Pattern Recognition and Machine Learning (Information Science and Statistics)," Springer-Verlag New York, Inc., Secaucus, NJ, USA., 2006.
[25] A. Alvarado, E. Agrell, D. Lavery, R. Maher, and P. Bayvel, "Replacing the soft-decision FEC limit paradigm in the design of optical communication systems," J. Lightw. Technol., vol. 33, no. 20, pp. 4338–4352, 2016.
[26] T. Koike-Akino, D.S. Millar, K. Kojima, and K. Parsons, "Coded modulation design for finite-iteration decoding and high-Dimensional modulation," in *Proc. Opt. Fiber Commun. Conf.*, Los Angeles, CA, USA, Mar. 2015, W4K1.
[27] E. Yamazaki et al.,"Fast optical channel recovery in field demonstration of 100-Gbit/s Ethernet over OTN using real-time DSP," Optics Express, 19, 2011, p. 13179.
[28] T. Koike-Akino et al., "Iteration-aware LDPC code design for low-power optical communications," J. Lightw. Technol., 2016 (pre-print available).
[29] K. Sugihara et al., "A spatially-coupled type LDPC code with an NCG of 12 dB for optical transmission beyond 100 Gb/s," in *Proc. Opt. Fiber Commun. Conf.*, Anaheim, CA, USA, Mar. 2013, OM2B4.

David S. Millar (S'07–M'11) received the M.Eng. degree in electronic and communications engineering from the University of Nottingham, Nottingham, U.K., in 2007, and the Ph.D. degree in Electronic and Electrical Engineering from University College London (UCL), London, U.K., in 2011.

His doctoral work was concerned with the development of equalization and modulation techniques for the mitigation of fiber nonlinearity in coherent optical transmission systems. He is currently a Principal Member of Research Staff at Mitsubishi Electric Research Laboratories (MERL) in Cambridge, Massachusetts, U.S.A. His research interests include coherent optical transmission systems, digital coherent receiver design, coded modulation for optical communications, and digital nonlinearity mitigation.

Dr. Millar has served as a Reviewer for several IEEE publications including IEEE Photonics Technology Letters, IEEE Journal of Selected Topics in Quantum Electronics, IEEE Communications Letters, and the IEEE/OSA Journal of Lightwave Technology. He is currently serving on the Technical Program Committee for the Optical Fiber Communications (OFC) Conference.

Robert Maher (M'09–SM'15) received the B.Eng. and Ph.D. degrees in electronic engineering from Dublin City University, Dublin, Ireland, in 2005 and 2009, respectively.

His doctoral research was focused on the development and characterization of cost-efficient wavelength tunable transmitters suitable for reconfigurable agile optical networks. In 2010, he received the IRC INSPIRE Marie Curie Fellowship and joined the Optical Networks Group at University College London (UCL), London, U.K. In 2013, he was appointed as a Senior Research Associate on the UNLOC EPSRC Program Grant, within the Optical Networks Group at UCL. His current research interests include spectrally efficient long-haul transmission for coherent optical networks, fiber nonlinearity mitigation techniques, and dynamic optical networking.

Dr. Maher is a Member of the Marie Curie Fellows Association.

Domaniç Lavery (S'09–M'13) received the M.Phys. degree in theoretical physics from the University of Durham, Durham, U.K., in 2009, and the Ph.D. degree in electronic and electrical engineering from University College London (UCL), London, U.K., in 2013.

His doctoral research was focused on the use of digital coherent transceivers and their application to spectrally efficient high-capacity passive optical networks. He is currently with the Optical Networks Group, UCL, as a Research Associate, investigating techniques for approaching channel capacity in nonlinear fiber transmission.

Dr. Lavery is a Member of the Optical Access Systems and Wireless Backhaul Networks subcommittee for the Optical Fiber Communication Conference (20152016) and was a Member of the technical programme committee for the 20th European Conference on Networks and Optical Communications. He received the IEEE Photonics Society Graduate Student Fellowship in 2012 and the Marconi Society's Paul Baran Young Scholar Award in 2013.

Toshiaki Koike-Akino (M'05–SM'11) received the B.S. degree in electrical and electronics engineering, M.S. and Ph.D. degrees in communications and computer engineering from Kyoto University, Kyoto, Japan, in 2002, 2003, and 2005, respectively.

During 2006–2010, he has been a Postdoctoral Researcher at Harvard University, and joined Mitsubishi Electric Research Laboratories, Cambridge, MA, USA, since 2010. His research interest includes digital signal processing for data communications and sensing.

Dr. Koike-Akino received the YRP Encouragement Award 2005, the 21st TELECOM System Technology Award, the 2008 Ericsson Young Scientist Award, the IEEE GLOBECOM'08 Best Paper Award in Wireless Communications Symposium, the 24th TELECOM System Technology Encouragement Award, and the IEEE GLOBECOM'09 Best Paper Award in Wireless Communications Symposium.

Milutin Pajovic (M'15) received the PhD degree in Electrical and Ocean Engineering from the Massachusetts Institute of Technology and Woods Hole Oceanographic Institution, in September 2014. He joined the Mitsubishi Electric Research Labs (MERL) in Cambridge, MA, in September 2014, where he is currently member of the research staff. His main research interests lie in the areas of signal processing, statistical inference and machine learning, applied to physical layer optical and wireless communications and indoor localization.

Alex Alvarado (S'06–M'11–SM'15) was born in Quellón, on the island of Chiloé, Chile. He received his Electronics Engineer degree (Ingeniero Civil Electrónico) and his M.Sc. degree (Magíster en Ciencias de la Ingeniería Electrónica) from Universidad Técnica Federico Santa María, Valparaíso, Chile, in 2003 and 2005, respectively. He obtained the degree of Licentiate of Engineering (Teknologie Licentiatexamen) in 2008 and his PhD degree in 2011, both of them from Chalmers University of Technology, Gothenburg, Sweden.

Dr. Alvarado is currently a Senior Research Associate at the Optical Networks Group, University College London, United Kingdom. In 2012–2014 he was a Marie Curie Intra-European Fellow at the University of Cambridge, United Kingdom, and during 2011–2012 he was a Newton International Fellow at the same institution. In 2008, he was holder of the Merit Scholarship Program for Foreign Students, granted by the Ministère de l'Éducation, du Loisir et du Sports du Québec. Dr. Alvarado is a recipient of the 2009 IEEE Information Theory Workshop Best Poster Award, the 2013 IEEE Communication Theory Workshop Best Poster Award, and the 2015 IEEE Transaction on Communications Exemplary Reviewer Award. His general research interests are in the areas of digital communications, coding, and information theory.

Milen Paskov (S'13–M'16) received a B.Sc. degree in electrical engineering and computer science in 2010 from Jacobs University Bremen, Germany. In 2011 he received a M.Sc. in spacecraft technologies and satellite communications from University College London (UCL), U.K. Between 2011 and 2015 he completed his Ph.D. work within the Optical Networks Group at UCL, U.K.

His research focused on digital signal processing algorithms for coherent optical systems and optical comb generation for optical superchannels. After his Ph.D. he spent 6 months with Mitsubishi Electric Research Laboratories (MERL), Cambridge, USA working on low complexity digital signal processing for next generation optical systems.

Dr. Paskov is a reviewer for IEEE Photonics Technology Letters, IEEE Photonics Journal and IEEE Transactions on Communications.

Keisuke Kojima (S'82–M'84–SM'13) was born in Hokkaido, Japan, in 1958. He received the B.S., M.S., and Ph.D. degrees in electrical engineering from the University of Tokyo, Tokyo, Japan, in 1981, 1983, and 1990, respectively. He also received the M.S. degree from the University of California, Berkeley, CA, USA, in 1982.

He worked for eight years at the Central Research Laboratory, Mitsubishi Electric Corp., from 1983 on the research of narrow linewidth lasers and AlGaAs/GaAs DFB and DBR lasers. He spent nine years at AT&T/Lucent Bell Laboratories on the R&D of uncooled Fabry–Perot and DFB lasers, vertical-cavity surface-emitting lasers, passive optical network systems, and metro optical systems, first as a Member of Technical Staff, and later as a Technical Manager. He also worked at Agere Systems, Denselight Semiconductors, and TriQuint Semiconductors on optical devices and modules, and optical systems testbed. He has been with Mitsubishi Electric Research Laboratories, Cambridge, MA, USA, since 2005, where he is currently working on the R&D of photonic-integrated circuits and coherent optical systems, as a Senior Principal Member Research Staff.

Dr. Kojima has more than 160 publications in journals and conference proceedings, and is a Fellow of the Optical Society of America.

Kieran Parsons (M'07–SM'09) received the B.Eng. and Ph.D. degrees in electronic and communications engineering from the University of Bristol, Bristol, U.K., in 1992 and 1996, respectively.

From 19972002, he was with Nortel Networks, Ottawa, Canada, where he worked on wireless and long-haul optical communications system architecture and design. From 2004–2006, he worked on carrier-grade mesh WiFi RF system design at BelAir Networks (now part of Ericsson) and from 2006–2009 on 10-G PHY device development with Applied Micro, both in Kanata, Canada. In 2009, he joined Mitsubishi Electric Research Laboratories, Cambridge, MA, USA, where he is currently Team Leader and Senior Principal Member Research Staff. His research interests include digital signal processing and coherent optical transmission systems.

Benn C. Thomsen (M'06) received the B.Tech. degree in optoelectronics and M.Sc. and Ph.D. degrees in physics from The University of Auckland, Auckland, New Zealand.

His doctoral research involved the development and characterization of short optical pulse sources suitable for high-capacity optical communication systems. He then joined the Optoelectronics Research Centre, Southampton University, U.K., as a Research Fellow in 2002, where he carried out research on ultrashort optical pulse generation and characterization, optical packet switching based on optically coded labels, and all-optical pulse processing. He joined the Optical Networks Group, University College London, London, U.K., in 2004, and held an EPSRC Advanced Fellowship from 2006 to 2011 and was appointed as a lecturer in 2007. He is currently a senior lecturer at UCL and his research focuses on optical transmission, physical-layer implementation of dynamic optical networking technology and the development of high capacity multimode fibre systems exploiting MIMO DSP.

Seb J. Savory (M'07–SM'11) received the M.Eng., M.A., and Ph.D. degrees in engineering from the University of Cambridge, U.K., in 1996, 1999, and 2001, respectively, and the M.Sc. (Maths) degree in mathematics from the Open University, Milton Keynes, U.K., in 2007.

His interest in optical communications began in 1991, when he joined STL (subsequently Nortel) in Harlow, U.K, Harlow. Having been sponsored by Nortel through his undergraduate and postgraduate studies, he rejoined the Harlow Laboratories in 2000. In 2005, he moved to UCL where he held a Leverhulme Trust Early Career Fellowship from 2005 to 2007, before being appointed as a Lecturer (2007), Reader (2012) and Professor (2015). During 2014/15 he held a RAEng / Leverhulme Trust Senior Research Fellowship and was a recipient of the RAEng Colin Campbell Mitchell Award in 2015. In October 2015 he was elected as a Fellow of Churchill College, Cambridge and in January 2016 moved to Cambridge as a University Lecturer.

Dr. Savory is the Editor-in-Chief of IEEE Photonics Technology Letters and serves on the Steering Committee of the Optical Fiber Communication conference having previously served as a General Chair (2015) and Program Chair (2013).

Polina Bayvel (S'87–M'89–SM'00–F'10) received her BSc (Eng) and PhD degrees in Electronic & Electrical Engineering from University of London, UK, in 1986 and 1990, respectively.

In 1990, she was with the Fiber Optics Laboratory, General Physics Institute, Moscow (Russian Academy of Sciences), under the Royal Society Postdoctoral Exchange Fellowship. She was a Principal Systems Engineer with STC Submarine Systems, Ltd., London, UK, and Nortel Networks (Harlow, UK, and Ottawa, ON, Canada), where she was involved in the design and planning of optical fibre transmission networks. During 1994-2004, she held a Royal Society University Research Fellowship at University College London (UCL), and in 2002, she became a Chair in Optical Communications and Networks. She is the Head of the Optical Networks Group (ONG), UCL which she also set up in 1994. She has authored or co-authored more than 300 refereed journal and conference papers. Her research interests include wavelength-routed optical networks, high-speed optical transmission, and the study and mitigation of fibre nonlinearities.

Prof. Bayvel is a Fellow of the Royal Academy of Engineering (FREng), the Optical Society of America, the UK Institute of Physics, and the Institute of Engineering and Technology. She was the recipient of the Royal Society Wolfson Research Merit Award (2007-2012), 2013 IEEE Photonics Society Engineering Achievement Award, and the 2014 Royal Society Clifford Patterson Prize Lecture and Medal. In 2015 she and 5 members of ONG received the Royal Academy of Engineering Colin Campbell Mitchell Award for their pioneering contributions to optical communications technology.